AD-A052 890 SCIENCE APPLICATIONS INC MCLEAN VA F/G 20/1
EXTENSIONS OF THE PARABOLIC EQUATION MODEL FOR HIGH-ANGLE BOTTO--ETC(U)
DEC 77 L B DOZIER, C W SPOFFORD N00039-76-C-0326
UNCLASSIFIED SAI-78-712-WA NL

END
DATE FILMED
5-78
DDC

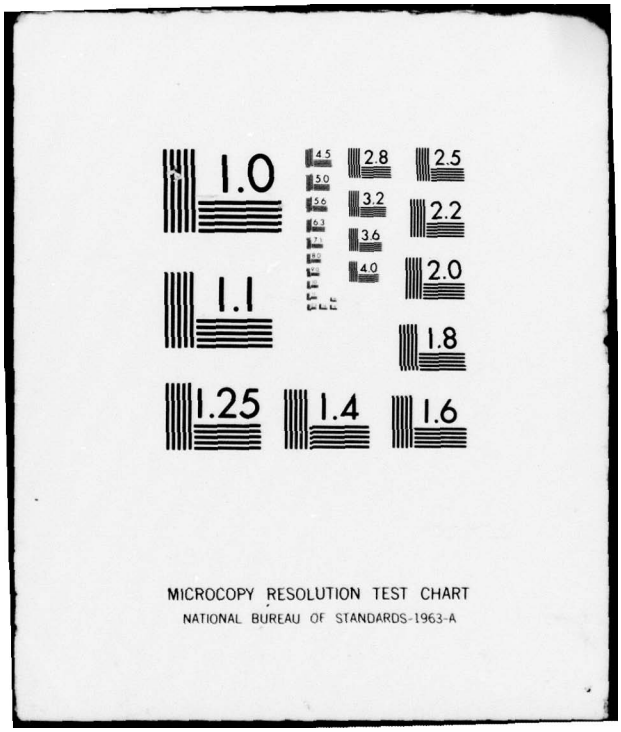
1.0
1.1
1.25
1.4
1.6
1.8
2.0
2.2
2.5
2.8
3.2
3.6
4.0
4.5
5.0
5.6
6.3
7.1
MICROCOPY RESOLUTION TEST CHART
NATIONAL BUREAU OF STANDARDS-1963-A

2

EXTENSIONS OF THE PARABOLIC EQUATION MODEL FOR HIGH-ANGLE BOTTOM-INTERACTING PATHS

SAI
ATLANTA • ANN ARBOR • BOSTON • CHICAGO • CLEVELAND • DENVER • HUNTSVILLE • LA JOLLA
LITTLE ROCK • LOS ANGELES • SAN FRANCISCO • SANTA BARBARA • TUSCON • WASHINGTON

EXTENSIONS OF THE PARABOLIC EQUATION MODEL FOR HIGH-ANGLE BOTTOM-INTERACTING PATHS

SAI-78-712-WA

31 December 1977

27 p.

Prepared for:
Naval Electronic Systems Command

Prepared by:
L. B. Dozier
C. W. Spofford

Prepared Under Contract No. N00039-76-C-0326

SCIENCE APPLICATIONS, INC.
8400 Westpark Drive, McLean, Virginia 22101
Telephone 703/821-4300

CONTENTS

Section 1
INTRODUCTION AND SUMMARY

1.1 Background

The parabolic-equation (PE) technique has proven to be a powerful tool in modeling propagation-loss under a variety of circumstances. Its fundamental limitation results from the parabolic or small-angle approximation employed in its derivation. While the approximation had been known for some time (Leontovich and Fock, 1946 and Fock, 1946), it became truly useful when integrated with the split-step FFT algorithm (Tappert and Hardin, 1973).

Strictly speaking, the approximation is not small-angle, but narrow-band. That is, the solution will be accurate for a small band of rays or modes with phase-velocities close to a selectable reference (e.g., McDaniel, 1975 or Fitzgerald, 1975). Since in underwater-sound applications small angles are nearly always of interest, this flexibility in selecting the accurate band offered very minimal improvements. As proposed by Fitzgerald (1975) one could solve a set of problems, each centered about different phase velocities, transferring energy between appropriate bands as indicated by a modal decomposition. While elegant, this solution requires solving for the normal-modes at each new environment and is probably impractical for most applications.

A similar type of approach has been proposed by Estes and Fain (1977) where each Fourier component is effectively propagated with refraction and reflection. A number

of approximations and assumptions are made in arriving at what appears to be a feasible implementation. The accuracy of the technique remains to be evaluated, as well as its practicality. It may, however, prove to be a useful reference or standard for comparison with approximate techniques even if it is found to be impractical for routine applications.

Other attempts at overcoming the small-angle limitation have included direct integration of the elliptic wave equation on very large, fast computers (e.g., Brock on NRL's TI-ASC, unpublished), and modification of the parabolic operator (Tappert, 1977). Brock's work is still in progress and may prove feasible for limited domains of high angles given such a powerful computer. Tappert has derived an operator which will accurately treat large angles and weak gradients, or small angles and strong gradients, but not large angles and strong gradients. More precise limits for this new operator have not been determined.

1.2 Approach and Summary

The work reported here represents an approximate solution to this last problem--large angles in the presence of strong gradients--formulated in a way to utilize the efficiency of the split-step FFT algorithm and hence to be applicable over large ranges. It is similar to the approximate solution developed to remove the bulk of the parabolic error for water-borne paths (Brock, Buchal, and Spofford, 1977). Their approach ("CMOD") was to transform the initial problem (specifically the sound-speed profiles) into a problem whose solution using PE would be much closer to the desired elliptic-equation solution of the original problem.

As is shown subsequently, this transformation breaks down (i.e., becomes double-valued) when applied to the strong gradients found in the refracting sediments of the ocean bottom. Fortunately, the principal CMOD objective--convergence zone spacings--is not relevant to the higher-angle bottom-bounce paths. For these paths a more appropriate constraint would be to preserve ray cycle distances or periods, thus ensuring that each ray would interact with the correct portion of the bottom and accumulate the right number of interactions at any given range.

It is possible to achieve this objective with controllable, small, errors so long as the bottom interaction process can be treated as refraction through strong-gradient sediments. This is typically the case in areas where the bottom is a good "reflector" such as abyssal plains. It would not apply to steep slopes of exposed basalt where the interaction process is, in fact, reflection.

Hence the specific problem of interest is the propagation of high angles over large distances where the energy is refracted in the ocean-bottom sediments (rather than reflected from a hard interface). The principal difficulty with PE in such geometries is that a steep angle effectively propagates with the period of a shallower angle since the horizontal component of its phase velocity is less than it should be. Hence the ray period, or cycle distance, is too large. For water-borne paths this problem was largely removed by CMOD. The relaxation of the CMOD convergence-zone constraint permits certain liberties to be taken with the sound-speed profile in the bottom which could not be considered in the water column.

For the bottom-interacting paths, a new algorithm, "BMOD," is proposed whose objective is to preserve ray periods given the user-specified sound-speed structure in the bottom. BMOD modifies the sound-speed profile in the bottom to compensate for the ray-period error accumulated in the water column. As a result, the impact of range-varying bathymetry and reflectivity is apparent on the correct rays, and mean levels may be accurately modeled. The position of a ray within the water column may, however, be in error at any one depth, but the error does not grow with range. Multipath interference effects in the field will have an inherent (but predictable) error since the phase velocities of the high-angle paths will still be incorrect.

The work reported here has focused on developing and testing the feasibility of this algorithm. Its full-scale implementation in a general PE code (with CMOD) was beyond the scope of the present effort. Such an implementation should present no major problems, and a number of associated issues are discussed in the final section of this report.

In summary, an algorithm has been developed which is able to modify ray periods in such a way that high-angle paths may be propagated in PE (via the split-step FFT algorithm) with sufficient accuracy to model many important bottom-related aspects of propagation loss. The algorithm requires no modifications to existing PE codes since it basically is used as a pre-processor of the environmental inputs.

1.3 Acknowledgments

This work was supported by the Naval Electronic Systems Command, Code 320 under Mr. W. Kamminga. The authors

are indebted to Dr. Fred Tappert of the Courant Institute (NYU) for several helpful discussions during the course of the work and and for making available to us some pre-publication manuscripts. At SAI the analysis of various parabolic operators by Mr. H. M. Garon provided substantial insight into this type of problem.

Section 2
THE ALGORITHM BMOD

In this section the basic algorithm, "BMOD," is developed. The previously developed water-column modification, "CMOD," is shown to fail when applied to the strong gradients formed in the ocean bottom. While it approximately conserves ray periods for water-borne paths, this was not its original intent--more emphasis being placed on mode turning points. Since we are not generally interested in sources or receivers deep in the bottom, the turning-point constraint can be removed, with ray periods becoming the principal concern.

2.1 Preserving Ray Periods

The CMOD algorithm approximately preserves the range variation of the true solution of the wave equation (WE), whereas PE errors accumulate with range. This becomes clear if we integrate the respective ray equations. Using Eqs. (C24) - (C26) of Ref. 1, for c = c(z) we have

$$\text{WE rays} \quad \frac{dr}{dz} = c\left(c_t^2 - c^2\right)^{-1/2} \tag{1}$$

$$\text{PECMOD rays} \quad \frac{dr}{dz} = \frac{1}{\sqrt{2}}\left(1 - \frac{c}{c_t}\right)^{-1/2}\left(1 - \frac{z}{2c}\frac{dc}{dz}\right) \tag{2}$$

$$\text{PE rays} \quad \frac{dr}{dz} = \frac{c_t}{c_o}\, c\left(c_t^2 - c^2\right)^{-1/2} \tag{3}$$

First, consider an ocean of constant sound speed gradient g and of infinite depth extending downward from z = 0. With $c(z) = c_0 + gz$, $g > 0$, the ray passing through z = 0 at an angle of θ from the horizontal turns at the depth $z_t = c_t - c_0/g$, where $c_t = c_0/\cos\theta$ is the sound speed at the turning point. For WE the range half-period is then

$$\Lambda_w(\theta) \equiv \int_0^{z_t} \frac{dr}{dz}\, dz = \frac{1}{g}\sqrt{C_t^2 - C_0^2} = \frac{C_0}{g}\tan\theta \qquad (4)$$

whereas for PECMOD we find

$$\Lambda_c(\theta) = \frac{\sqrt{\frac{C_t(C_t-C_0)}{2}}}{g} + \frac{C_0}{2\sqrt{2}\,g}\ln\left[\frac{\sqrt{C_t}+\sqrt{C_t-C_0}}{\sqrt{C_t}-\sqrt{C_t-C_0}}\right] \qquad (5)$$

$$= \frac{C_0}{g}\left\{\sqrt{S^2-1} - \sqrt{\frac{S(S-1)}{2}} - \frac{1}{\sqrt{2}}\ln\left[\sqrt{S}+\sqrt{S-1}\right]\right\}$$

where $s = \sec\theta = c_t/c_0$. Then the difference in range half-periods is

$$\Delta(\theta) \equiv \Lambda_w(\theta) - \Lambda_c(\theta)$$

$$\Delta(\theta) = \frac{1}{g}\sqrt{C_t - C_0}\left\{\sqrt{C_t+C_0} - \sqrt{\frac{C_t}{2}} - \frac{C_0}{4}\sqrt{\frac{2}{C_t-C_0}}\ln\left[\frac{\sqrt{C_t}+\sqrt{C_t-C_0}}{\sqrt{C_t}-\sqrt{C_t-C_0}}\right]\right\} \qquad (6)$$

$$= \frac{C_0}{g}\left\{\sqrt{S^2-1} - \sqrt{\frac{S(S-1)}{2}} - \frac{1}{\sqrt{2}}\ln\left[\sqrt{S}+\sqrt{S-1}\right]\right\}$$

Expanding the ln factor in terms of $\varepsilon \equiv \sqrt{(c_t - c_0)/c_t}$,

$$\Delta(\theta) = \frac{1}{g}\sqrt{c_t - c_o}\left\{\sqrt{c_t + c_o} - \sqrt{\frac{c_t}{2}} - \frac{c_o}{\sqrt{2\,c_t}}\right\} + \frac{1}{g}O(\varepsilon^2) \qquad (7)$$

Thus $\Delta(0) = 0$, and for small ε (small θ) it is clear that $\Delta(\theta) \geq 0$. For, consider the function

$$f(c) = \sqrt{c + c_t} - \sqrt{\frac{c_t}{2}} - \frac{c}{\sqrt{2c_t}} \qquad (8)$$

$$f'(c) = \frac{1}{2\sqrt{c+c_t}} - \frac{1}{\sqrt{2c_t}} > 0 \quad \text{for} \quad c > 0$$

Since $f(c_t) = 0$, $0 < c_0 < c_t$ implies $f(c_o) > 0$.

Moreover, if we consider the ratio

$$r_c(\theta) \equiv \frac{\Lambda_c(\theta)}{\Lambda_w(\theta)} = \sqrt{\frac{s}{2(s+1)}} + \frac{\ln\left[\sqrt{s} + \sqrt{s-1}\right]}{\sqrt{2(s^2-1)}}, \qquad (9)$$

then as $\theta \to \pi/2$, $r_c(\theta) \to 1/\sqrt{2} \simeq 0.707$ (the last term vanishes like $(\ln x)/x$ as $x = 4s \to \infty$). Thus, PECMOD <u>underestimates</u> the WE ray period by an increasing amount as θ increases from 0 to $\pi/2$, but never by more than 30%. For RR ray paths in the water column, the maximum error is much less. For example, Eq. (8) gives $r_c(16^o) = 0.9967$, i.e., an error of only 0.3%.

On the other hand, the usual PE algorithm <u>over-estimates</u> the WE ray period, and by a much larger amount than PECMOD underestimates it. From Eq. (3), the PE ray period is simply a factor of c_t/c_0 times the WE period; thus,

$$\Lambda_p(\theta) = \frac{c_t}{g c_0}\sqrt{c_t^2 - c_0^2} = \sec\theta \cdot \Lambda_w(\theta) \qquad (10)$$

The error in periods is

$$\Delta_p(\theta) \equiv \Lambda_p(\theta) - \Lambda_w(\theta) = \frac{1}{g}\sqrt{c_t^2 - c_0^2}\left(\frac{c_t}{c_0} - 1\right) \qquad (11)$$

As $c_t \to \infty$ ($\theta \to \pi/2$), $\Delta_p \to \infty$ and the error is unbounded. For $c_t \approx c_0$, the ratio of PECMOD error to PE error is (cf. Eq. (6))

$$E(\theta) \equiv \frac{\Delta(\theta)}{\Delta_p(\theta)} \approx \frac{1}{s-1}\left(1 - \sqrt{\frac{s+1}{2s}}\right) \qquad (12)$$

where $s = \sec\theta = c_t/c_0$. Thus, as $\theta \to 0$, $E(\theta) \to 1/4$. For very small angles, then, the PECMOD underestimate is about 1/4 of the PE overestimate, but this fraction rapidly decreases as θ increases. Returning to our earlier example, at $\theta = 16^\circ$ $\Lambda_p(\theta) = 1.040\Lambda_w(\theta)$ and hence $E(\theta) = 0.0033/0.040 \approx 0.08$.

Next, consider the typical case of a water column given by a piecewise linear sound speed profile with small gradients. The above analysis can be generalized to show that RR and RSR rays confined to the water column have a shorter period under PECMOD than under WE. This fact can now be used to our advantage.

The approach of BMOD is to replace a given ocean bottom and sound speed profile by a pseudo bottom composed of layers and a modified, piecewise-linear profile such that the period of the ray turning at the center depth of each layer is preserved. Extending CMOD directly into the bottom might appear to be an attractive solution. Since PECMOD underestimates ray periods in the water column, this modified bottom profile would, at least in the first few layers, actually have gradients <u>weaker</u> than the gradients at the same depth in the given bottom profile.

Unfortunately, this method fails because of a fundamental complication, namely the essential depth dependence of the CMOD algorithm. In fact, for deep bottom layers and large positive gradients, the CMOD depth transformation will become double-valued! The transformed depth coordinate $\tilde{z}$ is

$$\tilde{z} = z\, n^{1/2}(z) \tag{13}$$

where $n(z) = c_0/c(z)$ is the refractive index. For sufficiently large gradients, $n^{1/2}(z)$ will decrease faster than z increases, and multiple values of z will be mapped to the same $\tilde{z}$. Consider a bottom layer beginning with sound speed $\bar{c}$ at depth $\bar{z}$ and sound speed gradient g, i.e., $c(z)=\bar{c}+g(z-\bar{z})$, $z \geq \bar{z}$. If we solve the equation

$$\frac{d\tilde{z}}{dz} = n^{1/2}(z) + \frac{z}{2} n^{-1/2}(z)\, n'(z) = 0 \tag{14}$$

we find that $\tilde{z}$ will reach a maximum at $z = z^*$, where

$$z^* = \frac{2}{g}\left(\bar{z}g - \bar{c}\right), \tag{15}$$

and then $\tilde{z}$ will turn back on itself. Of course, only for sufficiently large g, namely

$$g > \frac{2\bar{c}}{\bar{z}} , \tag{16}$$

does $z^* > \bar{z}$ exist, which is why this problem never occurs in the water column. However, it can easily happen if we try to extend CMOD into the bottom. For example, consider a bottom layer beginning at $\bar{z}$ = 4,878 m with $\bar{c}$ = 1,524 m/sec. Then if g > 5/8 sec^{-1}, which is often true of real bottoms, CMOD fails. Thus, while CMOD is quite good for the water column ($n \approx 1$), it cannot handle both steep angles and $n \ll 1$.

Fortunately, the principal objective of CMOD--correct convergence-zone spacings--is not relevant to steep bottom-interacting paths. Our concern is to preserve ray periods, and we can achieve this by annexing a well-chosen bottom to the CMOD-transformed water column. The resulting problem is then solved using PE. The ray period for a bottom-interacting path is then found by integrating the PECMOD ray equation (2) through the water column and then the PE ray equation (3) through the bottom. For any given ray, the contribution from the water column is predetermined by CMOD, but BMOD then recursively modifies the sound speed gradient in each layer so that the period of the ray turning at the midpoint of the layer is preserved.

2.2 Formal Description of the Algorithm

Let the water column be composed of (N-1) layers such that $c(z) = c_i$ at the top $z = z_i$ of the i^{th} layer and

$c(z) = c_{i+1}$ at the bottom $z = z_{i+1}$, for i=1, ..., N-1. The reference sound speed is still denoted by c_0; in the following we assume c_0 is also the minimum sound speed, so that c_0 is invariant under CMOD. Let g_i be the gradient in the i^{th} layer, so that $c_{i+1} = c_i + g_i(z_{i+1} - z_i)$. At the bottom of the water column, $z = z_N$ and $c = c_N$. Let the bottom sound speed have a given gradient g, so that $c(z) = c_N + g(z - z_N)$ for $z > z_N$. (The extension to a general piecewise linear bottom is straightforward.) Now applying CMOD to the water column yields $\tilde{z}_i$ and $\tilde{c}_i$, i=1, ..., N. We extend this modified profile into the bottom by defining layer boundaries $\tilde{z}_{N+1}$, $\tilde{z}_{N+2}$, ... and gradients $\tilde{g}_N$, $\tilde{g}_{N+1}$, ... such that the period of the ray turning at the midpoint of each layer is preserved when PE is used to solve this pseudo problem.

The method of solution is recursive: first, $\tilde{g}_N$ is found; then, $\tilde{g}_{N+1}$ is found given that steep rays must pass through the layer with $\tilde{g}_N$, and so on. Thus, assume $\tilde{g}_i$, i=N, ..., M-1 have already been found. Let us reference rays in untransformed (not CMOD) space by their angle θ_0 at the sound channel axis z_0, or equivalently, by the sound speed $c_t = c_0/\cos\theta_0$ at their turning depth. Then W_v and W_b, the WE contributions to the ray half-period from the water column and bottom, respectively, are given by (cf. Eq. (4)).

$$W_w = \sum_{i=1}^{N-1} \frac{1}{g_i} \left\{ \sqrt{c_t^2 - c_i^2} - \sqrt{c_t^2 - c_{i+1}^2} \right\} \tag{17}$$

$$W_b = \frac{1}{g} \sqrt{c_t^2 - c_N^2} . \tag{18}$$

To compute the contribution C to the ray half-period from PECMOD, it is convenient to integrate in the untransformed space with its piecewise-linear profile. Just as in going from Eq. (2) to Eq. (5), we find

$$C = \sqrt{\frac{c_t}{2}} \sum_{i=1}^{N-1} \frac{1}{g_i} \left(\sqrt{c_t - c_i} - \sqrt{c_t - c_{i+1}} \right) \tag{19}$$

$$+ \sum_{i=1}^{N-1} \frac{c_i - g_i z_i}{2\sqrt{2}\, g_i} \ln \left[\frac{\sqrt{c_t} + \sqrt{c_t - c_i}}{\sqrt{c_t} - \sqrt{c_t - c_i}} \cdot \frac{\sqrt{c_t} - \sqrt{c_t - c_{i+1}}}{\sqrt{c_t} + \sqrt{c_t - c_{i+1}}} \right]$$

To compute the PE contribution P from the bottom layers previously defined by BMOD, we integrate Eq. (3) but in transformed space. With $\tilde{c}_i$, $N < i \leq M$, given by

$$\tilde{c}_i = \tilde{c}_{i-1} + \left(z_i - z_{i-1} \right) \tilde{g}_{i-1} \tag{20}$$

we obtain

$$P = \sum_{i=N}^{M-1} \frac{\tilde{c}_t}{c_0 \tilde{g}_i} \left\{ \sqrt{\tilde{c}_t^2 - \tilde{c}_i^2} - \sqrt{\tilde{c}_t^2 - \tilde{c}_{i+1}^2} \right\} \tag{21}$$

but now we must define $\tilde{c}_t$, the turning point speed of the transformed ray. Its initial angle $\tilde{\theta}_0$ at z_0 may be found from

$$\tan\tilde{\theta}_o = \frac{d\tilde{z}}{d\tilde{r}} = \frac{d\tilde{z}}{dr} = \frac{dz}{dr}\,\frac{d\tilde{z}}{dz} \qquad (22)$$

where dz/dr is obtained from Eq. (2), and dz̃/dz from Eq. (14). Thus,

$$\tan\tilde{\theta}_o = \sqrt{2\left(1-\frac{c_s}{c_t}\right)n_s} = \sqrt{2c_o\left(\frac{1}{c_s}-\frac{1}{c_t}\right)} \qquad (23)$$

Then the turning point speed $\tilde{c}_t$ is given by Snell's Law in the transformed medium:

$$\tilde{c}_t = \frac{c_o}{\cos\tilde{\theta}_o} \qquad (24)$$

Note that $\tilde{c}_t$ is <u>not</u> the same as the image of c_t under CMOD.

The final ingredient required to equate ray periods is the contribution from the current (M^{th}) layer. Assuming that $\tilde{c}_t > \tilde{c}_M$, the M^{th} layer with gradient $\tilde{g}_M$ will contribute

$$T = \frac{\tilde{c}_t}{c_o\tilde{g}_m}\sqrt{\tilde{c}_t^2-\tilde{c}_m^2} \qquad (25)$$

to the ray half-period. Then $\tilde{g}_M$ can be obtained by equating half-periods:

$$W_\omega + W_b = C + P + T \qquad (26)$$

or more explicitly,

$$\tilde{g}_M(\tilde{\theta}_0) = \frac{\tilde{c}_t\sqrt{\tilde{c}_t^2 - \tilde{c}_M^2}}{c_0\left(W_\omega + W_b - C - P\right)} \tag{27}$$

The problem now is to find the unique $\tilde{\theta}_0$ and $\tilde{g}_M$ such that Eq. (27) is satisfied and the turning depth

$$\tilde{Z}_t = \tilde{Z}_M + \frac{\tilde{c}_t - \tilde{c}_M}{\tilde{g}_M} \tag{28}$$

is also the midpoint $1/2(\tilde{z}_M + \tilde{z}_{M+1})$ of the next bottom layer. That is, we want

$$\Delta z(\tilde{\theta}_0) = \frac{\tilde{c}_t(\tilde{\theta}_0) - \tilde{c}_M}{\tilde{g}_M(\tilde{\theta}_0)} = \frac{1}{2}\left(\tilde{Z}_{M+1} - \tilde{Z}_M\right) \equiv D. \tag{29}$$

This transcendental equation for $\tilde{\theta}_0$ can be solved iteratively by the secant method. Let $\tilde{\theta}_0^{(i)}$, i=1, 2, ..., denote the sequence of iterates; corresponding anlges $\theta_0^{(1)}$ may be found by solving Eq. (23) for c_t and using Snell's Law. We choose

$$\tilde{\theta}_0^{(1)} = \cos^{-1}\left(\frac{c_0}{\tilde{c}_M}\right) \tag{30}$$

to be the initial angle of the ray which turns at the top of the layer; then $\Delta z(\tilde{\theta}_0^{(1)}) = 0$. Next, choose $\tilde{\theta}_0^{(2)}$ to be the initial angle of the ray which would turn at the midpoint of the current layer if the previous gradient were extended; i.e.,

$$\tilde{\theta}_0^{(2)} = \cos^{-1}\left[\frac{c_0}{\tilde{c}_M + \tilde{g}_{M-1}\left(\frac{\tilde{Z}_{M+1} - \tilde{Z}_M}{2}\right)}\right] \tag{31}$$

Then compute

$$\Delta z\left(\tilde{\theta}_0^{(2)}\right) = \frac{\tilde{c}_t\left(\tilde{\theta}_0^{(2)}\right) - \tilde{c}_M}{\tilde{g}_M\left(\tilde{\theta}_0^{(2)}\right)} \tag{32}$$

using Eq. (24) to obtain $\tilde{c}_t$, and Eq. (27) for $\tilde{g}_M$. Now the secant method consists of applying repeatedly the scheme

$$\tilde{\theta}_0^{(i)} = \tilde{\theta}_0^{(i-1)} + \frac{D - \Delta z\left(\tilde{\theta}_0^{(i-1)}\right)}{\tilde{\theta}_0^{(i-1)} - \tilde{\theta}_0^{(i-2)}}\left[\Delta z\left(\tilde{\theta}_0^{(i-1)}\right) - \Delta z\left(\tilde{\theta}_0^{(i-2)}\right)\right] \tag{33}$$

for i=3, 4, ..., and with D given by Eq. (29). The iteration terminates when

$$\left|\Delta z\left(\tilde{\theta}_0^{(i)}\right) - D\right| < \varepsilon D \tag{34}$$

for some tolerance factor ε chosen in advance; $\varepsilon = 0.01$ worked well in practice, and typically at most five iterations ($i \leq 5$) were required for convergence.

Finallly, $\tilde{g}_M$ is taken to be the gradient found on the last iteration. This algorithm could fail only if $W_w + W_b - C - P < 0$ for all $\tilde{\theta}_0 > \tilde{\theta}_0^{(1)}$, in which case it would be impossible to find a <u>positive</u> $\tilde{g}_M$ from Eq. (27). But in Section 2.1 we saw that $W_w + W_b - C > 0$ for all θ_0. Also, as $\tilde{\theta}_0 \to \pi/2$ ($\tilde{c}_t \to \infty$), $P \to 0$ in Eq. (20). Thus, for sufficiently large $\tilde{\theta}_0$, $W_w + W_b - C - P > 0$ and $\tilde{g}_M(\tilde{\theta}) > 0$, so there is no problem.

As a practical matter, it is good that at the bottom grazing angle, PECMOD underestimates the ray period. Thus, there is no initial angular gap (beyond the grazing angle) where ray periods cannot by preserved. Then by including enough bottom layers, the spacing of the angles where periods are preserved is narrow enough so that period errors at intermediate angles are small.

The generalization of the algorithm to the case of multiple bottom layers (gradients) in the given ocean is immediate.

Section 3
PE IMPLEMENTATION OF BMOD

In this section we present a PE implementation of BMOD for a homogeneous ocean and show that good results were obtained. We close with a discussion of some issues which would have to be addressed in a full implementation of BMOD in production PE codes.

3.1 Homogeneous Ocean

Although a full PE implementation of BMOD was beyond the scope of this contract, it was feasible to examine the simplest case of an isovelocity water column $c(z) \equiv c_0$, since then the CMOD transformation reduces to the identity map. The following such case was tested numerically: c_0 = 1524 m/sec, bottom sound speed gradient g = 0.5 sec^{-1}, source depth z_s = 12.2 m, water depth 3930 m, acoustic frequency 25 Hz, and a source aperture of 30^o.

The new PE source function of Garon, Hanna, and Rost (1977) was used to illuminate the desired angular aperture, beyond which the intensity fell off rapidly enough that, at least for the first ray period, the path of the steepest ray could be fairly well identified. Thus the ray period of the steepest ray could be well estimated from contour plots of the acoustic intensity produced by the PE runs.

The PE depth mesh interval was 45.7 m, and 2^7 mesh points were required. The BMOD-modified bottom sound-speed profile is shown in Table 1 at half-mesh intervals.

Table 1

MODIFIED BOTTOM SOUND SPEEDS (BMOD)

Depth (m)	Sound Speed (ft/sec)	Angle Preserved (deg)	Layer Gradient (sec^{-1})
3930.3	1524.4		
3953.2	1556.4	11.59°	1.402
3976.0	1588.5		
3998.9	1637.2	21.39°	2.134
4021.7	1686.0		
4044.6	1738.8	28.75°	2.312
4067.4	1791.7		

The midpoint of each layer is identified by the angle (in the water column) of the ray which turns there and whose period is preserved. Below the last depth shown a layer of constant sound speed was added to insure no steeper bottom returns. Now the WE period for a ray with angle θ_s in the water column is

$$\Gamma_w(\theta_s) = 2\left[\frac{H}{\tan\theta_s} + \frac{c_o}{g}\tan\theta_s\right], \qquad (35)$$

where H is the depth of the water column. The PE period for the same ray (unmodified profile) is then obtained merely by a multiplication:

$$\Gamma_p(\theta_s) = \frac{c_t}{c_o}\,\Gamma_w(\theta_s) = \sec\theta_s\,\Gamma_w(\theta_s) \qquad (36)$$

Thus we find

$$\Gamma_w(30^\circ) = 17.30 \text{ km}, \qquad \Gamma_p(30^\circ) = 19.99 \text{ km}$$

In the actual PE run with BMOD, the 30° period appeared to be about 17.6 km, or much closer to WE than to PE.

3.2 The General Inhomogeneous Case

The numerical testing of BMOD which fell within the scope of this contract has indicated its applicability to a more general class of inhomogeneous problems. As bottom gradients and water depths increase, however, we must expect that BMOD will become less efficient. For example, as the ratios of sound speeds at adjacent PE mesh points increase

(i.e., as bottom gradients increase), the split-step Fourier algorithm suffers more and more from aliasing; that is, the fraction of total energy which is aliased will grow. The only remedy for this problem is to increase the sampling in depth, i.e., to increase the number of depth mesh points. However, this doubly reduces computational efficiency: not only do the FFTs in depth take longer, but the range step Δr must be decreased.

Another possible limitation is that the PE depth mesh spacing controls the spacing of the angles of the rays whose periods are preserved. If that angular spacing gets too wide, significant errors in period could occur for intermediate angles.

If the modified gradients become too steep, the rays of interest will want to turn back up in the bottom almost instantaneously. Clearly, a ray which spends a horizontal distance less than Δr in the bottom cannot be treated accurately by PE. Taking Δr very small is computationally inefficient.

Finally, it appears feasible to extend BMOD to slowly varying range-dependent environments, but again, careful numerical testing would be required.

Section 4
CONCLUSION

We have presented a new algorithm BMOD for use in solving for acoustic pressure fields with significant energy returned from the ocean bottom. When combined with the previosly introduced CMOD, BMOD creates a pseudo-problem which, when solved by PE, should be a good approximation to the true WE solution for a certain class of problems. This class should be determined by a full PE implementation of BMOD, followed by numerical evaluation.

REFERENCES

H. K. Brock, R. N. Buchal, and C. W. Spofford, J. Acoust. Soc. Am. 62, 543-552 (1977).

L. E. Estes and G. Fain, J. Acoust. Soc. Am. 62, 38-43 (1977).

R. M. Fitzgerald, J. Acoust. Soc. Am. 57, 839-842 (1975).

V. A. Fock, J. Phys. USSR 10, 399-409 (1946).

H. M. Garon, J. S. Hanna, and P. V. Rost, "Construction of a New Source Function for the Parabolic Equation Algorithm," J. Acoust. Soc. Am. 61, S12(A).

M. A. Leontovich and V. A. Fock, J. Phys. USSR 10, 13-24 (1946).

S. T. McDaniel, J. Acoust. Soc. Am. 57, 307-311 (1975).

F. D. Tappert, "The Parabolic Approximation Method," in Lecture Notes in Physics No. 71, edited by J. B. Keller and J. Papadakis (Springer-Verlag, New York, 1977).

D. D. Tappert and R. H. Hardin SIAM Rev., 423(A) (1973).

Distribution List

ARPA Research Center
Unit 1
Moffett Field, CA 94035
ATTN: Dr. Theo Kooij

Naval Air Development Center
Department of the Navy
Warminster, PA 18974
ATTN: Mr. C. Bartberger

Naval Electronic Systems Command
Department of the Navy
Washington, D.C. 20360
ATTN: ELEX 03, Mr. J. Cybulski
PME-124/60, Dr. G. Hetland

Naval Surface Weapons Center
White Oak
Silver Spring, MD 20910
ATTN: Dr. I. Blatstein

Naval Ocean Research and
Development Activity
Department of the Navy
NSTL Station, MS 39529
ATTN: CAPT Hamilton, NOL
Dr. A. Anderson
Dr. J. Davis
CDR T. J. McCloskey
Dr. G. Hamilton
CDR G. Ranes
Dr. R. D. Gaul
CDR J. E. Paquin

Naval Research Laboratory
4555 Overlook Avenue, S.W.
Washington, D.C. 20375
ATTN: Dr. B. Adams
Mr. H. Brock
Dr. B. Hurdle
Dr. R. Ferris

Naval Intelligence Support
Center
4301 Suitland Road
Washington, D.C. 20390
ATTN: Dr. E. Bissett

Naval Ocean Systems Center
Department of the Navy
San Diego, CA 92152
ATTN: Dr. E. Tunstall
Dr. H. Schenck
Dr. H. Bucker
Mr. M. Pedersen

Naval Underwater Systems Center
New London Laboratory
New London, CT 06320
ATTN: Dr. H. Weinberg
Dr. F. DiNapoli

Office of Naval Research
Department of the Navy
800 N. Quincy Street
Arlington, VA 22217
ATTN: Dr. J. B. Hersey

Applied Physics Laboratory
The Johns Hopkins University
Johns Hopkins Road
Laurel, Maryland 20810
ATTN: Dr. G. Smith
Mr. A. Boyles

Applied Research Laboratory
University of Texas
P. O. Box 8029
Austin, TX 78712
ATTN: Dr. L. Hampton

Distribution List (Cont'd)

Bell Telephone Laboratories
1 Whippany Road
Whippany, NJ 07981
ATTN: Dr. V. Gianola

Bolt Beranek and Newman, Inc.
50 Moulton Street
Cambridge, MA 02138
ATTN: Dr. H. Heine

Catholic University
Department of Physics
Washington, D.C. 20064
ATTN: Dr. J. McCoy

ENSCO
Ocean System and Science Division
8001 Forbes Place
Springfield, VA 22201
ATTN: Dr. S. Schneider

University of Hawaii at Manoa
Hawaii Institute of Geophysics
2525 Correa Road
Honolulu, HI 96822
ATTN: Dr. M. Odegard

Institute for Acoustical Research
615 S.W. 2nd Avenue
Miami, FL 33130
ATTN: Dr. W. Jobst

Lamont-Doherty Geological
Observatory
Palisades, N.Y. 10964
ATTN: Dr. H. Kutschale

New York University
Courant Institute
251 Mercer Street
New York, N.Y. 10012
ATTN: Dr. F. D. Tappert

Penn State Applied Research
Laboratory
P. O. Box 30
State College, PA 16801
ATTN: Dr. S. McDaniel

Underwater Systems, Inc.
8121 Georgia Avenue
World Bldg.
Silver Spring, MD 20910
ATTN: Dr. M. Weinstein

University of Miami
School of Marine and
Atmospheric Sciences
10 Rickenbacker Causeway
Miami, FL 33149
ATTN: Dr. H. DeFerrari

Tracor, Inc.
Ocean Sciences Department
1610 Research Blvd.
Rockville, MD 20850
ATTN: Mr. R. Urick

Tracor, Inc.
6500 Tracor Lane
Austin, TX 78721
ATTN: Dr. A. Wittenborn

Woods Hole Oceanographic
Institution
Woods Hole, MA 02543
ATTN: Dr. R. Spindel

Defense Documentation Center
Bldg. 5, Cameron Station
Alexandria, VA 22314 2 cys